European ECOSTRESS Hub
Algorithm Theoretical Basis Document Land Surface Temperature

Reference: EEH-D4-ATBDLST

ESA Contract No. 4000129873/20/I-NS

Prepared by	Tian Hu, Martin Schlerf, Kaniska Mallick, Patrik Hitzelberger and Yoanne Didry (LIST)
Reference	EEH-D4-ATBDLST
Issue	1
Revision	0
Date of Issue	2021-05-21
Status	**Final Approved Version**

CHANGE LOG

Issue	Revision	Date	Author	Comment
1	0	2021-05-21	Hu, Schlerf, Mallick, Hitzelberger, Didry	Final version

Contents

Abstract

Land surface temperature (LST) is one of the most important state variables in the physical processes of surface energy and water balance from local to global scales and is the driving force in the land-atmosphere long-wave radiation and turbulent heat fluxes exchanges (Hu et al. 2019; Li et al. 2013; Mallick et al. 2014). Remote sensing remains the only avenue for obtaining spatially explicit LST over large regions with sufficiently high spatial and temporal resolutions. Given the direct linkage to LST via the radiative transfer process, thermal infrared remote sensing is widely used in LST estimation (Gillespie et al. 1998; Wan and Dozier 1996; Wang et al. 2019). The ECOsystem Spaceborne Thermal Radiometer Experiment on Space Station (ECOSTRESS) mission was selected as a NASA Earth-Ventures Instrument (EV-I) Class-D mission on the International Space Station (ISS). The instrument onboard includes a thermal infrared (TIR) multispectral scanner with five spectral bands operating between 8 and 12.5 µm, namely the space-ready Prototype HyspIRI Thermal Infrared Radiometer (PHyTIR). Starting from 2018, the TIR data has been acquired globally from the nominal International Space Station (ISS) altitude of 400 +/- 25 km at a spatial resolution of 38m x 69m with a swath width of 402 km (53°). Considering the unprecedentedly high spatial and temporal resolution, ECOSTRESS shows great promise in providing LST with pronouncedly improved performances, consequently facilitating monitoring plant-water dynamics and ecosystem changes with climate (Fisher et al. 2020). The overarching objective of the European ECOSTRESS Hub (EEH) is to develop LST and ET products for Europe and Africa using high spatial and temporal resolution information from multiple TIR bands of ECOSTRESS. To solve the ill-posed problem of LST inversion (more unknowns than measurements), various approaches have been developed. In the EEH, two different methods, i.e. the temperature emissivity separation (TES) algorithm and the split-window (SW) algorithm are adopted. This ATBD will elaborate on these two approaches, as well as the cloud mask at the beginning.

1. Introduction

Taking advantage of the TIR imager prototype HyspIRI Thermal Infrared Radiometer (PHyTIR) onboard the ISS, ECOSTRESS will investigate spatio-temporal dynamics of vegetation water stress through the measurement of LST (Fisher et al. 2020; Hulley et al. 2017). LST is the principal driving force in exchanging longwave radiation at the surface-atmosphere interface and is very sensitive to evaporative cooling and surface moisture variations (Hu et al. 2017; Hu et al. 2016; Hu et al. 2019; Mallick et al. 2015). It provides direct information on the land surface moisture status and surface energy balance partitioning (Kustas and Anderson 2009; Mallick et al. 2014). The overarching objective of the European ECOSTRESS Hub (referred to as EEH here after) is to develop LST and ET products for Europe and Africa using high spatial and temporal resolution information from multiple TIR bands of ECOSTRESS. Due to the unprecedented high spatial and temporal resolutions, new challenges are imposed with respect to:

1) Huge volume of generated remote sensing data and the limitations in the computational resources needed to process these data into derived products for the user community,

2) Uncertainties in different scientific algorithms for generating continental or global products,

3) Lack of universal consensus on the most suitable models under all sets of environmental, hydrological, and biome conditions.

From these challenges, there arises a demand for an ECOSTRESS hub to provide information from multiple models embedded in the hub where a range of conceptually different algorithms will be implemented in a cloud environment.

Different LST retrieval methods have been developed until now, including the single-channel algorithm, split-window (SW) algorithm and temperature-emissivity separation (TES) algorithm, among others (Li et al. 2013). Considering the multiple thermal bands available in the ECOSTRESS observations, the SW algorithm and the TES algorithm have been selected as the operational LST estimation methods in the EEH-LST module. Due to the strong attenuation of thermal infrared signal reaching the sensor by clouds or optically thick aerosol,

cloud screening is required to mask out the cloud-contaminated scenes before LST estimation can be further used (Shang et al. 2017).

This remaining part of this document will describe the theory and methodology first, then detail the process for cloud screening and the TES and SW algorithms, respectively.

2. Theory and basis

2.1. Thermal infrared (TIR) remote sensing background

In clear-sky conditions, the atmosphere can be regarded as horizontally homogeneous and isotropic. The top-of-atmosphere (TOA) spectral infrared radiance consists of six components:

1) surface thermal emittance L_1

$$L_1 = \tau_v(\lambda,\mu)\varepsilon(\lambda,\mu)B(\lambda,T), \tag{2.1}$$

2) thermal path radiance L_2

3) reflected atmospheric downwelling radiance by the surface L_3

$$L_3 = \tau_v(\lambda,\mu)\int_0^{2\pi}\int_0^1 \mu' f_r(\mu;\mu',\varphi')\, L_t^{\downarrow}(\lambda,-\mu',\varphi')d\mu' d\varphi', \tag{2.2}$$

4) reflected solar beam by the surface L_4

$$L_4 = \tau_v(\lambda,\mu)\tau_s(\lambda,\mu)\mu_0 E_0(\lambda) f_r(\mu;\mu_0,\varphi_0), \tag{2.3}$$

5) reflected solar diffuse radiation by the surface L_5

$$L_5 = \tau_v(\lambda,\mu)\int_0^{2\pi}\int_0^1 \mu' f_r(\mu;\mu',\varphi')\, L_s^{\downarrow}(\lambda,-\mu',\varphi')d\mu' d\varphi', \tag{2.4}$$

6) path radiance resulting from scattering of solar radiation L_6.

In the equations above, μ_0 and μ are the cosine of solar zenith angle and viewing zenith angle, respectively, φ_0 is the relative azimuth angle between the viewing angle and solar radiation, τ_v and τ_s are the transmittance at the viewing angle and solar angle, respectively, ε is the surface emissivity, f_r is the surface directional reflectance distribution function (BRDF), $B(\lambda, T)$ is the radiance emitted by a blackbody at surface temperature T, $E_0(\lambda)$ is the spectral solar irradiance incident on the top of the atmosphere (normal to the beam), $L_t^{\downarrow}$ and $L_s^{\downarrow}$ are the atmospheric downwelling radiance and solar diffusion radiation. The diagram for the radiative transfer process is displayed in Figure 2.1.

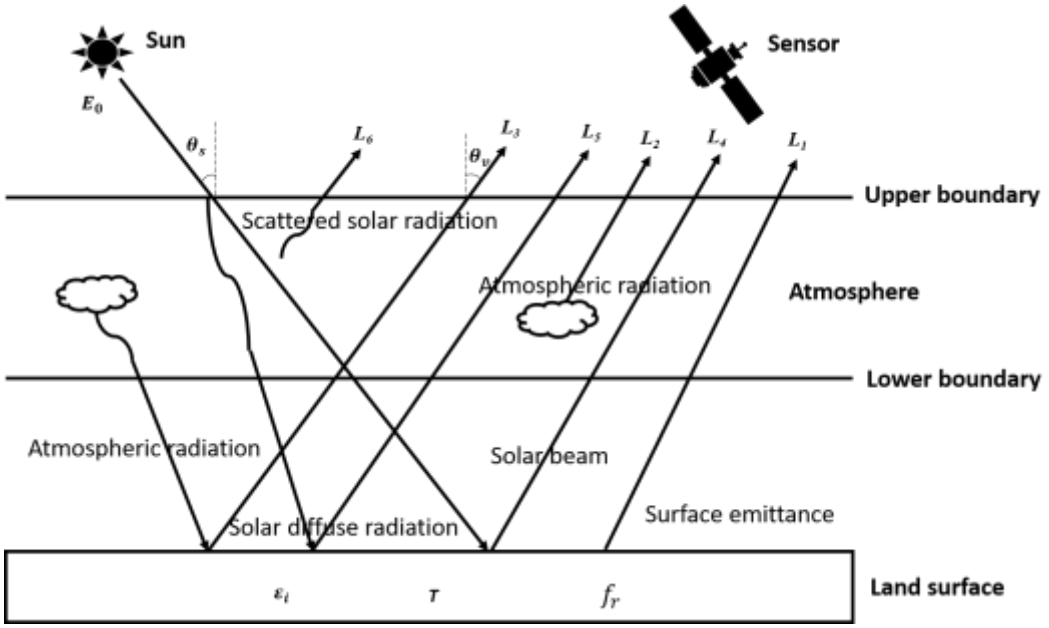

Figure 2.1. Illustration of radiative transfer process in the infrared regions.

In the thermal atmospheric window between 8 and 14 μm, the contribution from solar radiation is negligible. Thus, $L_4 - L_6$ are normally ignored in the radiative transfer process. Assuming the surface is Lambertian and with atmospheric upwelling radiance and downwelling radiance noted as $L_a{}^{\uparrow}$ and $L_a{}^{\downarrow}$, the thermal radiative transfer equation can be simplified to

$$L_\lambda = \tau_\lambda\left(\varepsilon_\lambda B(T,\lambda) + (1-\varepsilon_\lambda)L_a{}^{\downarrow}\right) + L_a{}^{\uparrow}. \quad (2.5)$$

where the at-sensor thermal signal L_λ only depends on surface temperature T, emissivity ε_λ, atmospheric transmittance τ_λ, and atmospheric upwelling and downwelling radiance. Among these variables, surface temperature and emissivity represent the surface properties, and the other three variables describe the thermal conditions of the atmosphere. Considering the spectral response function of the sensor, the radiative transfer equation needs to be convolved. However, it is inconvenient to use the convolved form of the radiative transfer equation in practice. Instead, the band-averaged variables are used to account for the spectral response function. The band-averaged thermal radiative transfer equation can be expressed as

$$L_i = \tau_i\left(\varepsilon_i B_i(T) + (1-\varepsilon_i)L_{ai}{}^{\downarrow}\right) + L_{ai}{}^{\uparrow}. \quad (2.6)$$

To remove the atmospheric attenuation effects and obtain the surface emittance from the at-sensor radiance, the three atmospheric components $L_{ai}^{\downarrow}$, $L_{ai}^{\uparrow}$ and τ_i need to be calculated using an atmospheric radiative transfer model driven by atmospheric profiles including air temperature and relative humidity at different atmospheric levels.

2.2. ECOSTRESS instrument characteristics

The ECOSTRESS instrument was implemented by placing the existing PHyTIR on the International Space Station (ISS), which was developed under the NASA Earth Science Technology Office (ESTO) Instrument Incubator Program (IIP). ECOSTRESS provides data with 38-m in-track and 69-m cross-track spatial resolution and predicted temperature sensitivity of ≤0.1 K. The ISS orbit allows excellent coverage of the selected targets including diurnal coverage. The detailed specifics of the radiometer are listed in Table 2.1. The spectral response functions of the five bands of ECOSTRESS are shown in Figure 2.2.

Table 2.1. ECOSTRESS Radiometer Characteristics (Hulley and Hook 2016b)

Description	Value	Unit	Notes
Spectral			
Measured band centres	Band 1 – 8.29*, Band 2 – 8.78, Band 3 – 9.20*, Band 4 – 10.49, Band 5 – 12.09	µm	* bands not available after May 15, 2019 will
Measured FWHM	Band 1 – 0.354, Band 2 – 0.310, Band 3 – 0.396, Band 4 – 0.410, Band 5 – 0.611	µm	
Radiometric			
Nominal radiometric accuracy at 300 K	0.5	K	typical value varies with wavelength of band
Nominal radiometric precision at 300 K	0.15	K	typical value varies with wavelength of band
Radiometric precision at 300 K per band	0.21, 0.13, 0.10, 0.10, 0.29	K	measure values (TVAC)
Number of blackbodies	2		one controlled between 16 ℃ and 24 ℃, one controlled to 46 ℃. The scanning sequence is hot bb, cold bb, earth scene repeating
Dynamic range	200 – 435	K	varies with spectral band, 12um band saturates at the highest temperature
Spatial			
Pixel size at nadir	69 × 38	m	2 pixels in cross track and 1 pixel in down track
Swath width	384	km	Varies with ISS height, assumes height of 400 km
Scene size	5400 × 5632	pixels	

Aperture size	200	mm	
Scan speed	25.4	rpm	
Scan angle	+/- 25	degrees	
Scene size	44	swaths	
Temporal			
Orbit crossing	multiple		per day
Global land repeat	multiple		per day
Data collection			
Temporal coverage	day and night		
Land coverage	land surface above sea level		
Water coverage	n/a		
Open ocean	n/a		

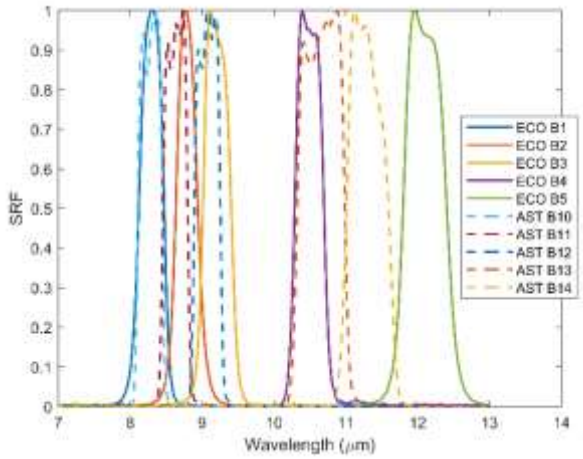

Figure 2.2. Spectral response function of ECOSTRESS TIR bands, along with the ASTER TIR bands. The ECOSTRESS and ASTER bands are denoted with ‘ECO’ and ‘AST’, respectively.

3. Cloud mask

In the cloud screening process, three calibrated ECOSTRESS thermal bands are used based on a multispectral clear sky-conservative thresholding approach. Discriminating cloud depends on both the characteristics of the clouds being detected and the land surface type below the clouds. Normally, clouds are brighter and colder than the land surface they obscure. However, surfaces covered by snow, ice and reflective sand may embody highly similar reflectance signatures to clouds, especially at higher elevations (Ackerman et al. 2010; Hulley and Hook 2008). As such, a scene-dependent approach for identifying clouds will be adopted (Hulley and Hook 2016a).

3.1. Inputs

The cloud masking approach will only use the calibrated, quality controlled TIR radiances (ECOSTRESS L1B product) as input considering only the TIR radiances are available for the ECOSTRESS radiometer.

3.2. Cloud masking procedure

In theory, the brightness temperature can be calculated using the radiance based on the Planck's function. However, the function will become inaccurate for a sensor's spectral response that deviates from the delta function behaviour. Instead, a look up table (LUT) is built to link the band-effective radiances convolved by the spectral response functions of ECOSTRESS with the brightness temperatures in 0.01 K intervals with the range of 150-380 K to cover the expected temperature range from very cold (e.g. cirrus clouds) to very hot (maximum surface temperature) image objects.

A two-step approach is adopted. The final cloud mask pixels are set if any of the individual tests detects cloud. Thus, this approach is deemed as a clear sky-conservative method.

3.2.1. Test on the 10.6 µm band

Clouds are normally colder than the land surface below (except for clouds over old background and low, warm summertime clouds). The cloud temperatures over land are usually

<300 K but change with time, land surface type and geolocation. In this test, a comprehensive LUT is compiled through simulations using RTTOV and MERRA2 atmospheric profiles, stratified by month, time of the day, emissivity and latitude/longitude.

3.2.2. Test on the difference between the 10.6 and 12 μm bands (thin cloud and cirrus)

This test works well for thin clouds, cirrus, the edges of thick clouds, low reflectance clouds and other types of cloud, by using the BT difference in the two split-window channels. The thresholds are listed in the table below, stratified by viewing zeniths angle (VZA) and the brightness temperature in Band 4.

Table 3.1. Threshold for the BT difference test

	$BT_{10.6-12}$ (K)				
	VZA (°)				
$BT_{10.6}$ (K)	44.5	38.6	29	14.9	≤ 3
≤ 260	0.58	0.58	0.59	0.59	0.59
270	0.65	0.66	0.66	0.67	0.68
280	0.97	0.94	0.90	0.88	0.87
290	4.4	4.0	3.6	3.4	3.3
300	8.1	7.8	7.2	6.8	6.6
310	10.8	10.8	10.8	9.8	9.6
400	8.6	8.7	8.9	8.7	8.7

3.2.3. Final cloud mask

After exercising the two tests above, the final cloud mask pixels are set if any of individual tests detect cloud, thus providing a clear-sky conservative cloud screening. Moreover, to detect the shadow of clouds, a cloud-growing method is implemented through extending each detected cloud pixel by an additional 3 pixels in a radial direction, and then using morphological infilling. The EEH cloud mask provides both the final cloud mask and the result for each step.

4. EEH temperature emissivity separation (TES) algorithm

The Advanced Spaceborne Thermal Emission and Reflection Radiometer (ASTER) Temperature Emissivity Working Group (TEWG) developed the hybrid TES algorithm by capitalizing on the strengths of multiple previous algorithms with additional features (Gillespie et al. 1998). The main advantage of the TES algorithm over others is that surface emissivity is estimated together with LST in the algorithm, without the requirement of prior emissivity estimates. The TES algorithm is applied to the surface-leaving TIR radiance that is obtained after removing the contributions of the atmospheric path radiance and transmittance to the at-sensor radiance at the top of atmosphere based on an atmospheric radiative transfer model driven by atmospheric profiles (Hulley and Hook 2016b). The diagram of the EEH-TES method is shown in Figure 4.1.

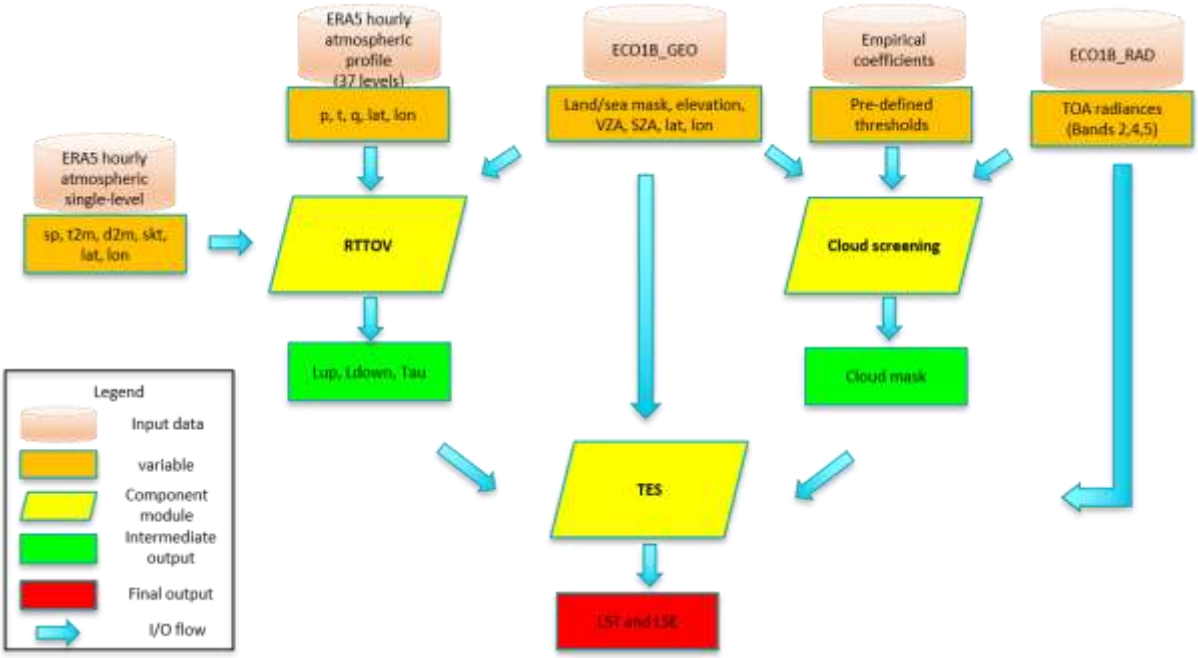

Figure 4.1. Flowchart of the EEH TES method, composed of two main parts, i.e. atmospheric correction and TES algorithm.

4.1. Atmospheric correction

The atmospheric correction is conducted by inputting atmospheric profiles into a radiative transfer model to obtain the three atmospheric parameters, i.e. path radiance, transmittance and downward sky irradiance. In the EEH, the RTTOV radiative transfer model

and the ERA5 atmospheric profiles will be used to obtain the atmospheric parameters due to the computation efficiency of RTTOV and high spatial and temporal resolutions of the ERA5 atmospheric data.

4.1.1. Atmosphere radiative transfer model

Two atmospheric radiative transfer models, i.e. Moderate Resolution Atmospheric and Transmittance Model (MODTRAN) and Radiative Transfer for TOVS (RTTOV) model, are widely used for atmospheric correction. Considering the computing efficiency, the RTTOV model is selected in the EEH, which is a very fast radiative transfer model for nadir-viewing passive visible, infrared and microwave satellite radiometers, spectrometers and interferometers (Saunders et al. 1999). It is written in FORTRAN 90 for simulating satellite at-sensor radiances, designed to be incorporated within user applications. Given an atmospheric profile of temperature, water vapour and, optionally, trace gases, aerosols and hydrometeors, together with surface parameters and a viewing geometry, RTTOV computes the top of atmosphere radiances in each of the channels of the sensor being simulated. Users can specify the channels to be simulated.

4.1.2. Atmospheric profiles

Currently, there are two options for atmospheric profiles available: 1) interpolation of data assimilated from Numerical Weather Prediction (NWP) models and 2) retrieved atmospheric geophysical profiles from remotely sensed observations. The NWP models use current weather conditions, observed from various sources (e.g., radiosondes, surface measurements and weather satellite observations) as input to dynamic mathematical atmosphere models to predict the weather. Examples include the Global Data Assimilation System (GDAS) product provided by the National Centres for Environment Prediction (NCEP), the Modern Era Retrospective-analysis for Research and Applications (MERRA) product provided by the Goddard Earth Observing System Data Assimilation System Version 5.2.0 (GEOS-5.2.0) and the European Centre for Medium-range Weather Forecasting (ECMWF) ERA5 hourly product. The reanalysis data are typically output in 6-hour increments, e.g., 00, 06, 12 and 18 UTC. In comparison, remote sensing data are available real-time, typically twice

daily and for clear-sky conditions. Examples of remote sensing data include the Atmospheric Infrared Sounder (AIRS) product and the Moderate Resolution Imaging Spectroradiometer (MODIS) product. However, the spatial coverage of remote sensing data is limited due to the availability only under clear sky.

In EEH, the ECMWF ERA5 product on single levels and on pressure levels are selected as input atmospheric data to the RTTOV model, describing the near-surface and atmospheric conditions, respectively (Table 4.1). The ERA5 hourly products are first linearly interpolated in time to the ECOSTRESS observation using the atmosphere data before and after the observation time. Then, the atmosphere data are interpolated spatially to the ECOSTRESS pixels using the bilinear interpolation method. The input variables required by RTTOV and related ERA5 data sets are correspondingly listed in Table 4.1.

Table 4.1. Geophysical variables available in the ERA5 reanalysis data

Geophysical fields		**Mandatory for RTTOV**	**Available in ERA5?**	**Remarks**
time	time	yes	yes	interpolated to the ECOSTRESS observation time
lat	latitude	yes	yes	interpolated to the ECOSTRESS pixels
lon	longitude	yes	yes	interpolated to the ECOSTRESS pixels
p	pressure	yes	yes	ERA5 data on 37 pressure levels
t	air temperature	yes	yes	ERA5 data on 37 pressure levels
q	specific humidity	yes	yes	ERA5 data on 37 pressure levels
sp	surface pressure	yes	yes	ERA5 data on single levels
skt	skin temperature	yes	yes	ERA5 data on single levels
t2m	temperature at 2 m	yes	yes	ERA5 data on single levels
d2m	specific temperature at 2 m	yes	yes	ERA5 data on single levels, dew point temperature is converted to specific humidity
lsm	land/sea mask	yes	no	from ECOSTRESS L1A GEO data
el	elevation	yes	no	from ECOSTRESS L1A GEO data
tcw	total column water	no	yes	added to L2 data for users' reference
Spatial resolution: 0.25° × 0.25°				
Temporal resolution: 1 hr reanalysis from 00:00 UTC				

4.2. TES method

The TES method has been described in detail in Hulley and Hook (2016b). The TES algorithm estimates temperature and emissivity spectrum by combining the NEM, the ratio and the minimum-maximum difference (MMD) modules. The NEW module is used to estimate temperature and iteratively remove the sky irradiance. From the calculated surface emittance, the emissivity spectrum is estimated. The ratio module calculates the ratio of the emissivity spectrum to the averaged emissivity. Through the ratioing, the shape of the emissivity spectrum is preserved but not the amplitude. To obtain the amplitude information, the minimum emissivity is calculated based on the regressed relationship between the minimum emissivity and MMD. Based the correct emissivity spectrum, a final LST can be calculated using the maximum emissivity and the corresponding surface emittance. The flowchart of the TES algorithm is shown in Figure 4.2.

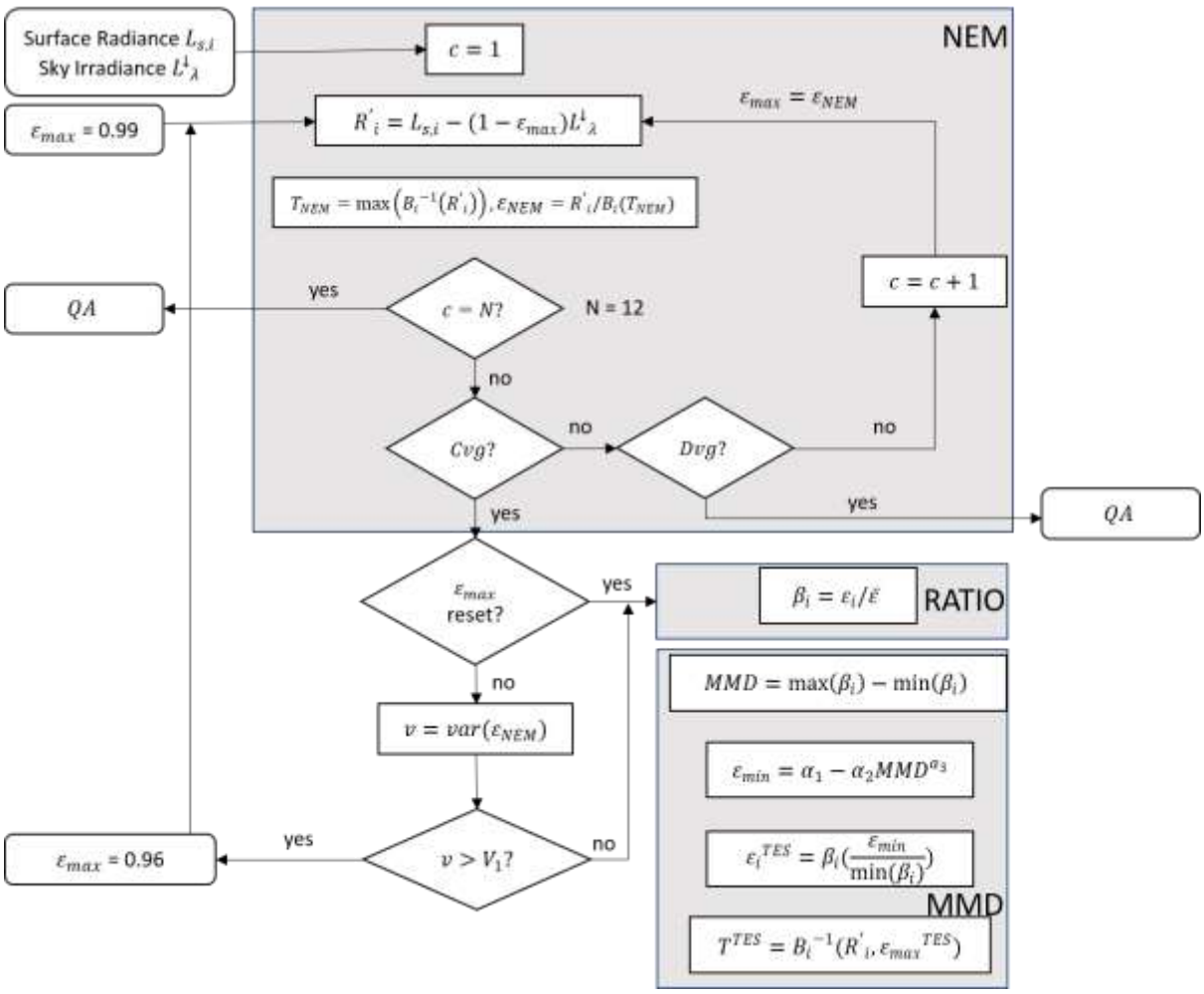

Figure 4.2. Flowchart of the TES algorithm, including the NEM, RATIO and MMD modules. Cvg = Convergence, Dvg = Divergence (modified from Hulley and Hook (2016b)).

4.2.1. NEM module

In the NEM module, the initial emissivity ε_{max} is used for all the bands. The role of NEM is to compute the surface kinetic temperature and a correct shape for the emissivity spectrum. An initial value of 0.99 is set for ε_{max}, which is typical for graybody such as vegetated surfaces, snow and water. However, this initial value is too high for non-graybody surfaces. Thus, if the variance of emissivity for ε_{max} = 0.99 is greater than V_1 (1.7×10^{-4}), then the pixel is assumed to consist of geologic materials. For geologic materials such as rocks and sand, ε_{max} is reset to 0.96 and the NEM module is executed again.

The first step in the NEM module is to estimate the surface emittance by removing the reflected sky irradiance from the surface-leaving radiance. The NEM temperature T_{NEM} is then calculated by inverting the Planck function for each band using ε_{max} and the surface emittance and taking the maximum of these temperatures considering the maximum temperature will be closest to the actual surface temperature if uncompensated atmospheric impacts exist. The NEM emissivity spectrum is then calculated as the ratio of surface emittance to that of a blackbody emittance with the temperature T_{NEM}. The new emissivity spectrum is then used to recalculate surface emittance, and the process is repeated until convergence, which is determined if the change in surface emittance between steps is less than the radiance equivalent to NEΔT (0.007 $W.m^{-2}.sr^{-1}.\mu m^{-1}$). The NEM module execution is stopped if the number of iterations exceeds the limit (set to12). The execution is also aborted if the slope of R'_i versus iteration c increases such that

$$\left|\frac{\Delta^2 R'}{\Delta c^2}\right| > t_1 \tag{4.1}$$

where t_1 is also set to radiance equivalent to NEΔT. The NEM module is stopped if, for any iteration, the emissivity spectrum falls out of the reasonable range (0.5, 1).

4.2.2. Ratio module

In the ratio module, the NEM emissivities are ratioed to their average value to calculate a β spectrum. Typical ranges for the β spectrum are between 0.75 and 1.32, given the typical emissivities range from 0.7 to 0.99.

4.2.3. MMD module

In the MMD module, the β emissivities are scaled to an actual emissivity spectrum using the regressed relationship between the spectral contrast (MMD) and the minimum emissivity ε_{min} determined from lab measurements of a variety of different spectra, including rocks, soils, vegetation, water and snow/ice. From ε_{min}, the actual emissivity spectrum can be found by re-scaling the β spectrum.

It is noted that for pixels with low spectral contrast such as graybody surfaces, the accuracy of MMD calculated is compromised and approaches a value depending on measurement error and residual error from incomplete atmospheric correction. For ECOSTRESS with a NEΔT <0.1 K, the measurement error is expected to be minimal and atmospheric correction residuals contribute the most to the MMD error. A further problem for graybody surfaces is a loss of precision because in the power-law curve of ε_{min} vs. MMD small changes in MMD can lead to large changes in ε_{min} at low MMD values.

After obtaining the emissivity spectrum, LST is calculated using the retrieved maximum emissivity and the corresponding atmospherically corrected radiance by inverting the Planck function.

4.3. TES sensitivity analysis

To analyse the accuracy and sensitivity of TES algorithm, a simulation dataset was compiled using the SeeBor V5.0 radiosonde database (Borbas et al. 2005). The database consists of 15704 global profiles of temperature, moisture and ozone at 101 pressure levels for clear-sky conditions. The profiles are taken from NOAA-88, an ECMWF 60L training set, TIGR-3, ozone sonders from 8 NOAA Climate Monitoring and Diagnostics Laboratory (CMDL) sites, and radiosondes from 2004 in the Sahara Desert (Figure 4.3). Quality checks were exercised to all the profiles based on the following criteria: for clear-sky conditions, the relative

humidity must be <99% at each level below 250 hPa; the original top of sounding pressure should be no greater than 30 hPa for temperature and moisture profiles and 10 hPa for ozone. A technique to extend the temperature, moisture and ozone profiles above the level of existing data that insures physically consistent behaviour near the top of the troposphere was implemented. Additionally, for each profile in the data set a physically based characterization of the surface skin temperature and surface emissivity are assigned.

There are 9136 profiles over land, which are selected in the simulation data. The numbers of daytime and night-time profiles are 4948 and 4188, respectively, based on the local sunrise and sunset times. The bottom atmospheric temperature (T_0) ranges between 200.2 and 318.5 K, and the water vapor content (WVC) varies from 0.1 to 7.8 g/cm^2.

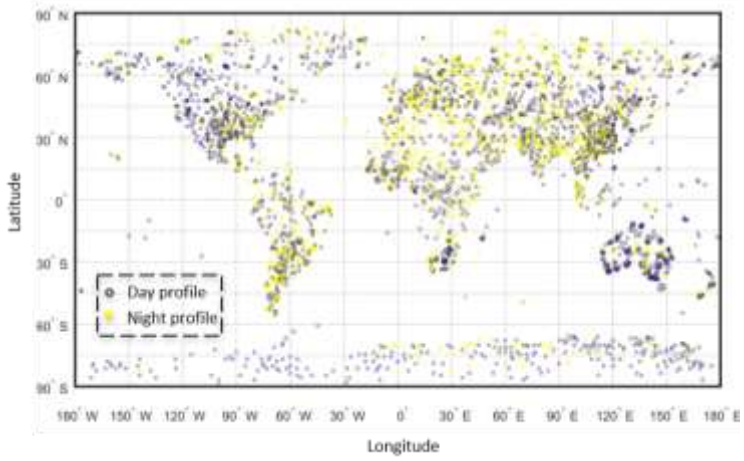

Figure 4.3. Global distribution of SeeBor 5.0 radiosonde database for both daytime and night-time.

The surface emissivity is described using the ASTER emissivity library including both natural and man-made materials (Baldridge et al. 2009). The library is a collection of contributions in a standard format with ancillary data from the Jet Propulsion Laboratory (JPL), Johns Hopkins University (JHU) and the United States Geological Survey (USGS). The ASTER library provides a comprehensive collection of over 2300 spectra a wide variety of materials covering the wavelength range between 0.4 and 15.4 µm. In the simulation dataset, 81 emissivity samples were selected, representing both vegetated and barren surfaces, water and snow/ice (Figure 4.4).

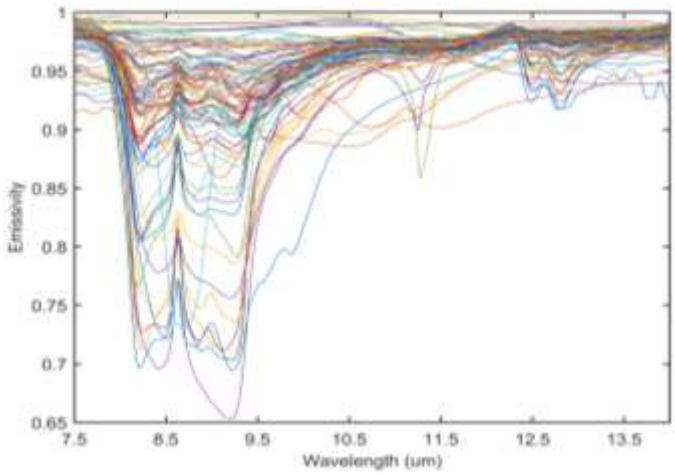

Figure 4.4. ASTER emissivity library, including 81 samples for sand, soil, vegetation, water, ice and snow.

The estimation uncertainty of the TES algorithm itself is shown in Figure 4.5. This analysis was conducted by taking the simulated surface-leaving radiance and atmospheric downwelling radiance (9136×81 = 740,016 cases) as inputs to the TES algorithm. The emissivity and temperature retrievals were compared with the surface emissivity and temperature used in the forward simulation. Thus, the atmospheric impacts were excluded. It can be found that the TES algorithm has high accuracy, with RMSEs of 0.01 and 0.40 K for emissivity and temperature estimates, respectively. The biases for both emissivity and temperature estimates are close to 0.

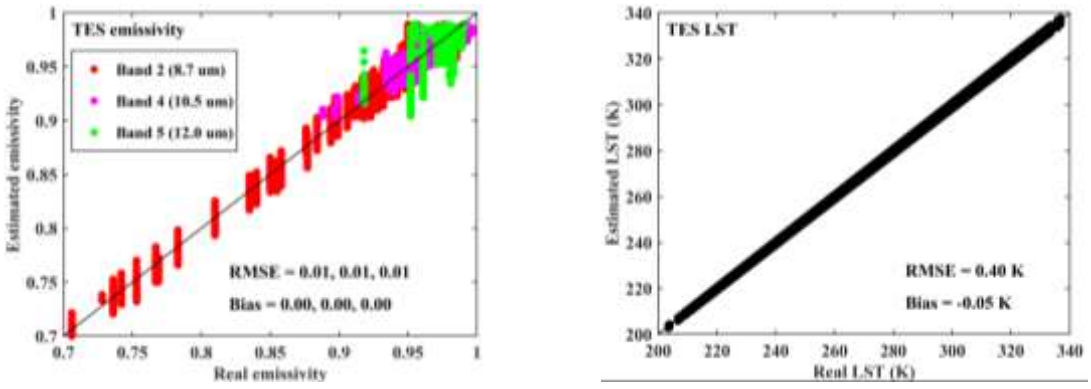

(a) emissivity (b) temperature

Figure 4.5. Uncertainty of the TES algorithm without atmospheric correction impacts. The emissivity and temperature used in the forward simulation are treated as the ‘ground truth’.

Normally, it is known that 10% change in water vapor content results in 2.1% change in radiance and 1 K change in atmospheric temperature leads to 1.3% change in radiance. To analyse the atmospheric correction impacts to the emissivity and temperature estimates,

noises were added to all the three bands used in the TES algorithm. The sensitivity of emissivity and temperature to atmospheric correction residuals is shown in Figure 4.6. The estimation uncertainties in both emissivity and temperature increase sharply with noises in surface-leaving radiances. When the noise exceeds 2%, the accuracy of LST will be lower than 1 K, and that of emissivity will be lower than 0.01. Therefore, the performance of TES algorithm is expected to be quite good in relatively dry atmosphere but degraded in humid atmosphere.

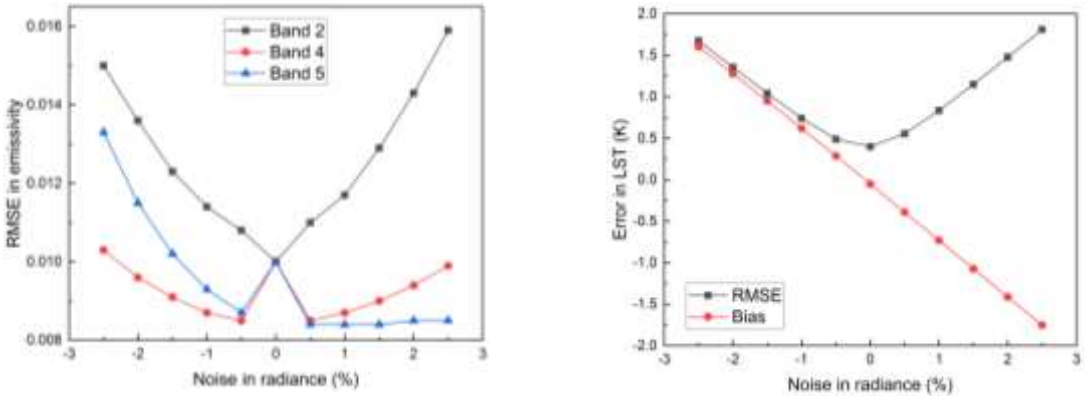

(a) emissivity (b) temperature

Figure 4.6. Sensitivity of emissivity and temperature estimates to atmospheric correction impacts. The atmospheric correction impact is depicted by adding noise at different magnitudes to surface-leaving radiance in all the three bands.

4.4. TES quality control and diagnostics

The temperature and emissivity products will be assessed using a set of quality control (QC) flags. These flags will depend on ECOSTRESS radiance quality, whether the pixel is over land or water, the atmospheric transmittance and cloud cover. The performance information in each step of the TES algorithm will also be provided in the QC flags to give users a summary of algorithm statistics. The QC flags are described using a 16-bit QC data. The structure of the QA data plane consists of six primary fields, which are detailed in Table 4.2:

1. Mandatory QC flags: overall description of status of pixel, produced with good quality, unreliable quality, not produced due to cloud or other reasons than cloud.

2. Data quality field: good data, missing strip data and filled in, missing strip data and not filled in, not seen

3. Cloud mask and land/water mask field.

4. The status of the NEM module: convergence, divergence, iteration number exceeding the limit, calculated emissivity out of the normal range.

5. Atmospheric transmittance.

6. MMD: MMD <0.03 (near-graybody), MMD >0.03 (containing bare soil).

Pixels with unreliable quality are typically either affected by cloud or high atmospheric water vapor content. These pixels usually have the emissivity in Band 5 < 0.95, or atmospheric transmittance <0.3.

Table 4.2. Bit flags defined in the QC data for the EEH-TES method

Bits	Long name	Description
1&0	Mandatory QA flags	00 = Pixel produced, best quality 01 = Pixel produced, nominal quality. Either one or more of the following conditions are met: 1) emissivity in both bands 4 and 5 < 0.95, i.e. possible cloud contamination 2) low atmospheric transmittance due to high water vapor content (<0.4) 3) pixel falls on missing scan line in Bands 1 and 5 and are filled using spatial neural network. 10 = Pixel produced, but cloud detected 11 = Pixel not produced due to missing data
3&2	Radiance data quality flag	00 = good quality L1B radiance data 01 = missing stripe pixel and filled in 10 = missing stripe pixel and not filled in 11 = not seen
5&4	Cloud mask and land/water mask	Not set. Check the L1B GEO and cloud mask products for this information
7&6	NEM module status	00 = convergence 01 = divergence 10 = iteration number exceeding the limit 11 = calculated emissivity out of the normal range
9&8	Atmospheric transmittance	00 = ≥0.8 01 = ≥0.7 10 = ≥0.4 11 = <0.4 (low transmittance)
11&10	MMD	00 = >0.15 (most silicate rocks) 01 = 0.1 – 0.15 (rocks, sand and some soils) 10 = 0.03 – 0.1 (mostly soils, mixed pixel) 11 = <0.03 (vegetation, water, ice and snow)
15 – 12	Not set	These four bits are reserved for additional information.

4.5. TES uncertainty estimation

Well-defined uncertainty statistics in the TES LST&E products are important for a better use of the data. A thorough understanding of the LST&E uncertainties will enhance the

usefulness of these data in surface energy balance, land surface and climate models. The Temperature Emissivity Uncertainty Simulator (TEUSim) has been developed by Hulley et al. (2012) for simulating LST&E uncertainties from various sources of errors for the TES algorithm in a rigorous manner. The error sources mainly include random errors (sensor noise), algorithm (model) and atmospheric correction (Hulley and Hook 2016b).

Similar to the simulation process in the TES sensitivity analysis (Section 4.3), the RTTOV atmospheric radiative transfer model is used for the simulations with a global set of SeeBor V5.0 radiosonde database and surface emissivity library, representing a wide range of atmospheric conditions and land surface types. To simulate the errors in the atmospheric profiles, a linearly decreasing temperature noise from 4 K at the surface to 2 K at 700 mb, and a constant 2 K above 700 mb were added to the temperature profiles at each level of the RTTOV profiles. The errors were generated using a random number generator with a mean centred on the uncertainties mentioned above. The humidity profiles were adjusted by scaling factors ranging from 0.8 to 1.2 using a uniformly distributed random number generator. The total LST uncertainty for the TES algorithm can be calculated as

$$\delta LST_{TES} = [\delta LST_M{}^2 + \delta LST_A{}^2 + \delta LST_N{}^2]^{1/2} \quad (4.2)$$

where δLST_M is the model error due to assumptions made in the TES calibration curve, δLST_A is the atmospheric error, and δLST_N is the error associated with measurement noise. These three error sources are assumed to be independent.

To calculate the separate contributions from each of these errors, the simulated atmospheric parameters and TOA radiance are denoted as x = [$\tau_\lambda(\theta)$, $L^{\uparrow}_\lambda(\theta)$, $L^{\downarrow}_\lambda(\theta)$] and y = $L_\lambda(\theta)$. In the estimation, some errors are normally associated with the calculated atmospheric parameters and observed TOA radiance, written as $\hat{x} = x + \delta x$ and $\hat{y} = y + \delta y$. The model error, δLST_M, due to assumptions in the TES algorithm, is written as

$$\delta LST_M = E[(f(x,y) - LST_{sim})^2|_{x,y}]^{1/2} \quad (4.3)$$

where LST_{sim} is the LST used in the simulation process, $E[.|_{x,y}]$ denotes the mean square error between the retrieved LST and that used in the forward simulation for inputs *x* and *y*. The atmospheric error can be written as

$$\delta LST_A = E[(f(\hat{x}, y) - f(x, y))^2|_{x,y}]^{1/2}. \quad (4.4)$$

The error caused by measurement noise can be written as

$$\delta LST_N = E[(f(x, \hat{y}) - f(x, y))^2|_{x,y}]^{1/2}. \quad (4.5)$$

The measurement noise is added to the TOA radiance directly using a random number generator with a mean centred on the ECOSTRESS NE∆T. Since the TES algorithm retrieved LST and LSE simultaneously, the above error equations can also apply to the emissivity retrieval for each band.

To calculate the estimation error for each pixel, the uncertainty is parameterized using viewing zenith angle, total water vapor content and land surface type using a least square method to fit a quadratic function. Three surface types are classified, i.e. grey body, transitional and bare. The transitional surface represents a mixed cover type and is calculated by varying the fractional vegetation cover f_v by 25%, 50% and 75% for the set of bare surface spectra (rocks, soils and sand) as follows:

$$\varepsilon_{trans} = \varepsilon_{gray}.f_v + \varepsilon_{bare}(1 - f_v), \quad (4.6)$$

where $\boldsymbol{\varepsilon}_{trans}$ is the transition emissivity, $\boldsymbol{\varepsilon}_{gray}$ is a gray body emissivity spectrum, and $\boldsymbol{\varepsilon}_{bare}$ is the bare surface emissivity spectrum. The total uncertainty for ECOSTRESS LST can be expressed as

$$\delta LST = a_0 + a_1 TCW + a_2 VZA + a_3 TCW.VZA + a_4 TCW^2 + a_5 VZA^2 \quad (4.7)$$

where δLST is the LST uncertainty calculated as the difference between the simulated and retrieved LST, a_i are the LST regression coefficients depending on surface types (gray body, transitional surface and bare surface). Similarly, the band emissivity uncertainties can be expressed as

$$\delta\varepsilon_i = b_{i,0} + b_{i,1} TCW + b_{i,2} VZA + b_{i,3} TCW.VZA + b_{i,4} TCW^2 + b_{i,5} VZA^2. \quad (4.8)$$

where $\delta\varepsilon_i$ is the band emissivity uncertainty between the input emissivity from emissivity spectrum library and the retrieved emissivity, $b_{i,j}$ are the LSE regression coefficients.

In the application of this uncertainty simulator, the emissivity in ECOSTRESS Band 2 is used to assign the coefficients of different land surface types to pixels accordingly. The emissivity thresholds used are ε < 0.85 for bare surface, 0.85 < ε < 0.95 for transitional surface and ε > 0.95 for grey body.

4.6. TES algorithm output

The TES temperature and emissivity products will be archived in Hierarchical Data Format 5 – Earth Observing System (HDF5-EOS) format files. The scientific variable arrays in the EEH-TES product are listed in Table 4.3, including descriptions of data type, units, valid range, fill value, scale factor and offset. The variables include LST and estimated error, emissivity for the 3 bands used and associated errors, QC data plane and precipitable water vapour content. The data types and scaling factors have been optimized to minimize the amount of memory required to store the data.

Table 4.3. The scientific data sets (SDSs) for the EEH-TES product

SDS	Long name	Data type	Unit	Valid range	Fill value	Scale factor	Offset
LST	land surface temperature	unit16	K	7500-65535	0	0.02	0.0
LST_Err	land surface temperature error	unit8	K	1-255	0	0.04	0.0
Emis2	Band 2 emissivity	unit8	n/a	1-255	0	0.002	0.49
Emis4	Band 4 emissivity	unit8	n/a	1-255	0	0.002	0.49
Emis5	Band 5 emissivity	unit8	n/a	1-255	0	0.002	0.49
Emis2_Err	Band 2 emissivity error	unit16	n/a	0-65535	0	0.0001	0.0
Emis4_Err	Band 4 emissivity error	unit16	n/a	0-65535	0	0.0001	0.0
Emis5_Err	Band 5 emissivity error	unit16	n/a	0-65535	0	0.0001	0.0
QC	Quality control for LST and emissivity	unit16	n/a	0-65535	0	n/a	n/a
PWV	Precipitable water vapor	unit16	cm	0-65535	0	0.001	0.0

5. EEH split window (SW) algorithm

Taking advantage of the different atmospheric absorption in two adjacent channels centred around 11 and 12 μm, the SW algorithm has been applied to many types of satellite data, including the Advanced Very Hight Resolution Radiometer (AVHRR), Moderate Resolution Imaging Spectrometer (MODIS), Spinning Enhanced Visible and Infrared Imager (SEVERI) and Geostationary Operational Environmental Satellites (GOES) (Gao et al. 2013; Hu et al. 2019; Wan and Dozier 1996; Yu et al. 2008). In the SW algorithm, land surface emissivity (LSE) is specified *priori* to disentangle the coupling between LST and LSE. LST is calculated directly from the TOA radiance using a polynomial with regressed coefficients. The diagram of the EEH-SW method is shown in Figure 5.1.

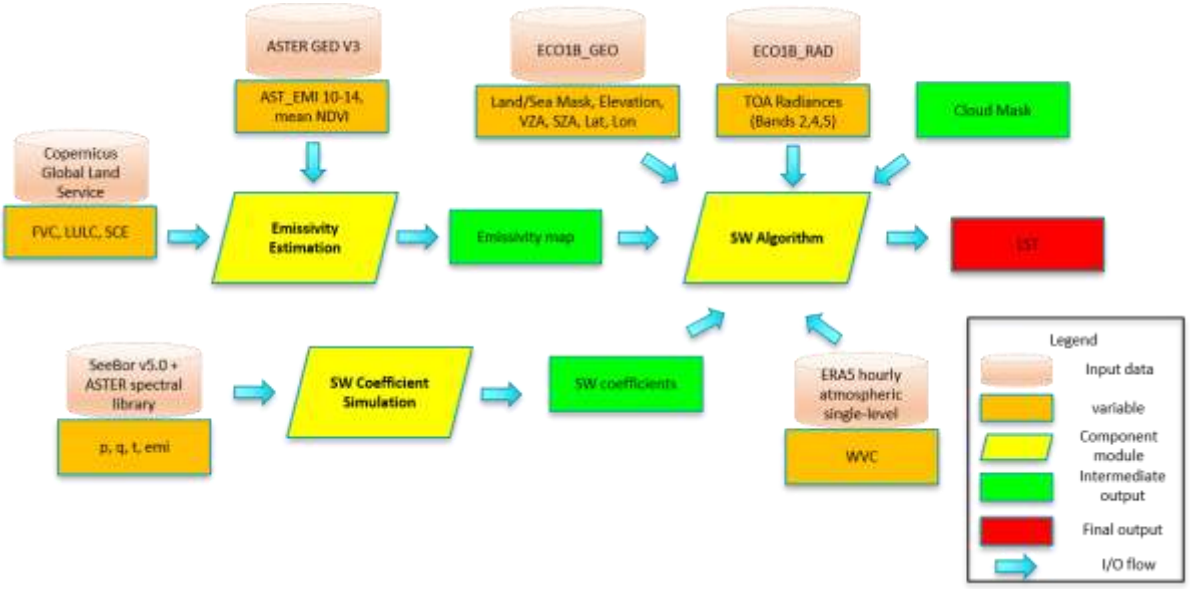

Figure 5.1. Flowchart of the EEH SW method, composed of two main parts, i.e. emissivity estimation and SW algorithm.

5.1. Emissivity estimation method

Prior information of LSE is necessary for the ill-posed problem of inversing temperature from multi-band radiances using the SW algorithm. Two types of empirical approaches are widely used for LSE estimation. The first type is the classification-based method, which was used in the MODIS LST product (Snyder et al. 1998). LSEs for each pixel in the two SW channels are estimated by assigning fixed values based on the land cover type and adjusted

based on the seasonal factors such as vegetation senescence and snow cover. The static emissivities for different surface types were calculated by combining various spectral component measurements with structural factors. However, large biases can be introduced into the LSE estimation due to the heavy dependence on the land surface classification products, which can have large uncertainties in heterogeneous landscapes. In particular, the assumption of a constant emissivity over barren surfaces is unrealistic considering the pronounced variations in emissivity for different soils, rocks and sand (García-Santos et al. 2015). The other one is the normalized difference vegetation index (NDVI)-based method (Sobrino et al. 2001; Valor and Caselles 1996), which assigns emissivity to pixels based on their NDVIs. For vegetated pixels, the emissivities are calculated using a linear weighted summary of the component soil and vegetation emissivities based on the fractional vegetation cover (FVC). The vegetation and soil emissivities are determined using the emissivity spectra in the spectral libraries. However, a constant value for the soil component emissivity degrades the accuracy of estimated emissivity (Li et al. 2019).

In the EEH-LST algorithm, the enterprise LSE estimation method based on the ASTER GED v3 product is used to provide emissivity (Yu et al. 2017b). The ASTER GED product is the average emissivity from 2000 to 2008 estimated from the ASTER observations based on the TES algorithm (Hulley et al. 2015). In this scheme, the land surface is classified into three classes, including permanent snow/ice, vegetation/soil mixed surfaces and inland water (Malakar et al. 2018; Yu et al. 2017b). The bare soil climatology is calculated from the ASTER GED data and the corresponding NDVI data attached. Corresponding adjustments are exercised over these different land surface types on the bare soil climatology (Figure 5.2).

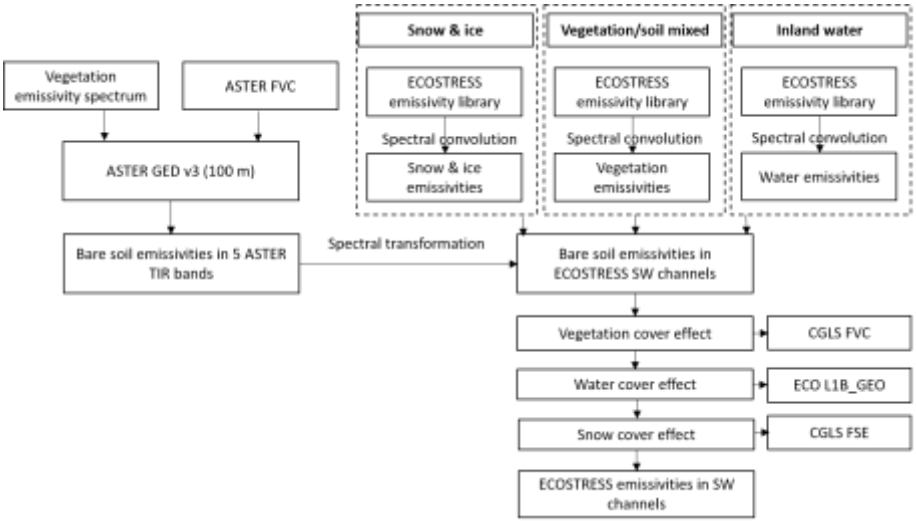

Figure 5.2. Flowchart of the LSE estimation process

5.1.1. Calculation of the bare soil emissivity climatology

The bare soil emissivity background information is extracted from the ASTER GED product first for the ECOSTRESS SW channels. The ASTER GED emissivity can be expressed as

$$\varepsilon_{i,ASTER} = \varepsilon_{i,bare}(1 - f_{ASTER}) + \varepsilon_{i,veg} f_{ASTER} \quad (5.1)$$

where $\varepsilon_{i,ASTER}$ is the ASTER GED emissivity of a partially vegetated pixel, $\varepsilon_{i,bare}$ and $\varepsilon_{i,veg}$ are the component emissivities of bare soil and vegetation, respectively, f_{ASTER} is the fractional vegetation cover of the ASTER pixel. Based on this equation, the bare soil emissivity component can be obtained as

$$\varepsilon_{i,bare} = \frac{\varepsilon_{i,ASTER} - \varepsilon_{i,veg} f_{ASTER}}{1 - f_{ASTER}} \quad (5.2)$$

where f_{ASTER} can be estimated calculated from the mean NDVI data in the ASTER GED v3 product as

$$f_{ASTER} = 1 - \frac{NDVI_{max} - NDVI}{NDVI_{max} - NDVI_{min}} \quad (5.3)$$

where $NDVI_{max}$ and $NDVI_{min}$ are set to 0.75 and 0.05, respectively (Sobrino et al. 2016). The vegetation component emissivities are obtained from the ECOSTRESS emissivity library and convolved using the ASTER spectral response function, which are 0.985, 0.983, 0.981, 0.981, 0.981 in ASTER Bands 10 - 14.

After the bare soil component emissivities in the five ASTER thermal bands are obtained, a linear conversion is conducted as follows

$$\varepsilon_{i,ECO\_B} = c_0 + c_1\varepsilon_{10,AST\_B} + c_2\varepsilon_{11,AST\_B} + c_3\varepsilon_{12,AST\_B} + c_4\varepsilon_{13,AST\_B} + c_5\varepsilon_{14,AST\_B} \quad (5.4)$$

where ε_{i,ECO_B} is the bare soil emissivity in the ECOSTRESS SW channels, ε_{10,AST_B} to ε_{14,AST_B} are the bare soil emissivities in the five ASTER TIR channels obtained from Eq. 5.2, c_0 to c_5 are the coefficients determined by linear regression using the ECOSTRESS emissivity library. Since this conversion is specifically for bare soil, a spectral set of soil, rocks and a few construction materials including asphalt and concrete are selected from the ECOSTRESS emissivity library for the regression. Both the source and target channel emissivities are convolved using the corresponding spectral response functions. The regressed coefficients are listed in Table 5.1. Considering the ECOSTRESS and ASTER channel positions (Figure 2.2), ASTER Bands 4 and 5 are used for ECOSTRESS Band 4 due to the adjacency, and all the five ASTER bands are used for ECOSTRESS Band 5 considering the little overlap of this band with any ASTER band. This is also reflected in the correlation coefficients and RMSEs, where the conversion to ECOSTRESS Band 4 is better comparatively. However, the conversion to ECOSTRESS Band 5 is still of high accuracy, with R^2 of ~0.9 and RMSE of ~0.001.

Table 5.1. Coefficients of the spectral conversion from ASTER to ECOSTRESS for bare soil emissivity

	c_0	c_1	c_2	c_3	c_4	c_5	R^2	*RMSE*
ECO B4	-0.0587	--	--	--	1.1359	-0.0768	0.9671	0.0011
ECO B5	0.2044	0.0453	0.0585	-0.1584	0.2294	0.6204	0.8809	0.0012

5.1.2. Adjustment over vegetation/soil mixed surfaces

To consider the annual and inter-annual variabilities in plant phenology and vegetation density, the emissivity over vegetation/soil mixed surface is described as

$$\varepsilon_i = \varepsilon_{i,ECO\_B}(1 - f) + \varepsilon_{i,ECO\_V} f \quad (5.5)$$

where ε_i is the emissivity of vegetation/soil mixed pixel, f is the FVC, ε_{i,ECO_V} is the vegetation emissivity in the ECOSTRESS SW channels, which are calculated using the ECOSTRESS emissivity library by averaging band-effective emissivities of selected vegetation types and set as 0.981 and 0.982 for Bands 4 and 5, respectively. Since no visible and near infrared bands

are available for the ECOSTRESS data, the FVC data from the Copernicus Global Land Service (CGLS) are used instead.

5.1.3. Adjustment over water covered surfaces

The inland water emissivity spectra in the ECOSTRESS spectral library are convolved to the ECOSTRESS SW channels and averaged among all selected samples (set as 0.989 and 0.985 for Bands 4 and 5, respectively). The water emissivity is then assigned directly to pixels classified as inland water using the land fraction dataset in the ECOSTRESS L1B_GEO data.

5.1.4. Adjustment over snow/ice covered surfaces

Snow with distinct emissivity spectral characters is a common natural phenomenon in the middle and high latitude regions in winter, which may impact the surface emissivity dramatically. Similar to the adjustment over vegetated surfaces, the CGLS fractional snow extent (FSE) data are used to adjust for snow/ice coverage. The permanent snow/ice emissivities are extracted from the ECOSTRESS emissivity library and convolved to the ECOSTRESS SW channels (set as 0.994 and 0.977 for Bands 4 and 5, respectively). The snow cover adjustment is conducted after the vegetation and water adjustment.

5.2. SW method

Multiple SW algorithms have been developed based on the differential atmospheric absorption in the two adjacent channels centred around 11 and 12 μm (Wan 2014; Wan and Dozier 1996). Basically, these methods can be divided into two categories: one expresses emissivity implicitly using different coefficient sets for different land surface types; the other category incorporates emissivity explicitly (Yu et al. 2017a). It was reported that significant uncertainties can be introduced into a surface-type dependent algorithm due to the misclassification in land surface type products and the intra-class variability in emissivity. The emissivity explicit algorithm is preferred, which allows for improvements in input emissivity to be directly translated into improved LST accuracy and enables easy incorporation of updated emissivity maps (Sobrino et al. 2016).

The EEH-LST algorithm follows the generalized SW method proposed by Wan and Dozier (1996) as follows:

$$T_s = b_0 + \left(b_1 + b_2\frac{1-\varepsilon}{\varepsilon} + b_3\frac{\Delta\varepsilon}{\varepsilon^2}\right)\frac{T_{11}+T_{12}}{2} + \left(b_4 + b_5\frac{1-\varepsilon}{\varepsilon} + b_6\frac{\Delta\varepsilon}{\varepsilon^2}\right)\frac{T_{11}-T_{12}}{2} \quad (5.6)$$
$$+ b_7(T_{11}-T_{12})^2$$

where T_s is the LST (in K), T_{11} and T_{12} are at-sensor brightness temperatures (in K) centred around 11 and 12 µm, respectively, $\boldsymbol{\varepsilon}$ is the mean emissivity of the SW channels, $\Delta\boldsymbol{\varepsilon}$ is the emissivity difference between the SW channels, and b_0 to b_7 are the algorithm coefficients.

5.2.1. Coefficient regression

To obtain the eight coefficients in Eq. 5.6, a simulation dataset is compiled using the RTTOV 12 atmospheric radiative transfer model and the SeeBor V5.0 atmospheric profile database. The atmospheric transmittance and the atmospheric upwelling radiance at viewing zenith angle from nadir to 35° with an increment of 5° and the atmospheric downwelling radiance at 53° are simulated for the SW channels for all the 9136 profiles over land. The numbers of daytime and night-time profiles are 4948 and 4188, respectively. WVC is divided into six subranges with an overlap of 0.5 g/cm^2: [0, 1.5], [1, 2.5], [2, 3.5], [3, 4.5], [4, 5.5] and [5, 7.8]. To maximize the algorithm performance over a wide range of surface conditions, the LST in the simulation is set as follows. For cold atmospheric profiles (T_0 < 280 K), the LST varies from T_0 - 20 K to T_0 + 4 K in steps of 5 K, and for warm atmospheric profiles (T_0 > 280 K), LST varies from T_0 - 5 K to T_0 + 29 K in steps of 5 K. In addition, a total of 81 emissivity spectra are selected from the ECOSTRESS spectral library, which include vegetation, water, ice, snow, rock, sand, and soil spectra. Finally, for given LST, LSE, and atmospheric parameters, the TOA radiances in ECOSTRESS Bands 4 and 5 are simulated using the radiative transfer equation (Equation 2.6), and the brightness temperatures are then calculated. Once the simulation database is established, the coefficients in Equation 5.6 can be determined via statistical regression.

5.2.2. LST estimation

After acquiring the emissivity for each pixel in the image and the algorithm coefficients stratified by VZA and WVC, LST can be calculated directly from the TOA radiances for clear-sky scenes screened using cloud mask. The WVC information is obtained from the ERA5 hourly single level data and interpolated temporally and spatially to ECOSTRESS pixels as described in Section 4.1.2.

5.3. SW sensitivity analysis

As conducted in Section 4.3, the sensitivity analysis for the SW method is also implemented using the same simulation data. The RMSE of LST estimates without emissivity estimation uncertainties, i.e. using the emissivities in the simulation data, is shown in Figure 5.3. The RMSE increases sharply with WVC, and the changes for the daytime and night-time are very similar. For small VZAs (<15°), the RMSE remains below 1 K. However, the RMSE increase above 1 K for large VZAs in humid atmosphere (WVC >4 cm).

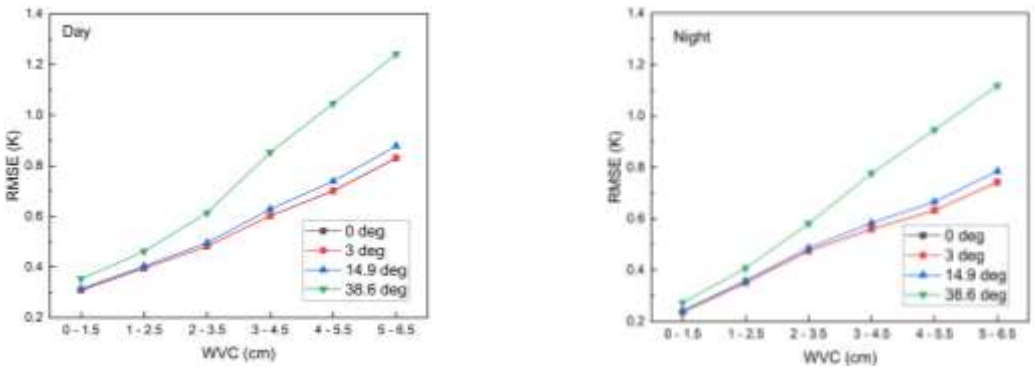

(a) daytime (b) night-time

Figure 5.3. RMSE of LST estimates using the SW method without emissivity estimation uncertainties for changing WVC and different view zenith angles during (a) daytime and (b) night-time.

The LST RMSE with emissivity noises at different magnitudes is shown in Figure 5.4. The RMSE for most cases is below 1 K when the noise in emissivity is below 0.1. Whereas, when the noise in emissivity is above 0.1, the RMSE for most cases is above 1 K, especially with large VZAs and in humid atmosphere. Thus, the estimation accuracy of LSE is vital for the LST estimation using the SW algorithm. To achieve an accuracy of 1 K for LST estimates, the estimation accuracy of LSE needs to be <0.01.

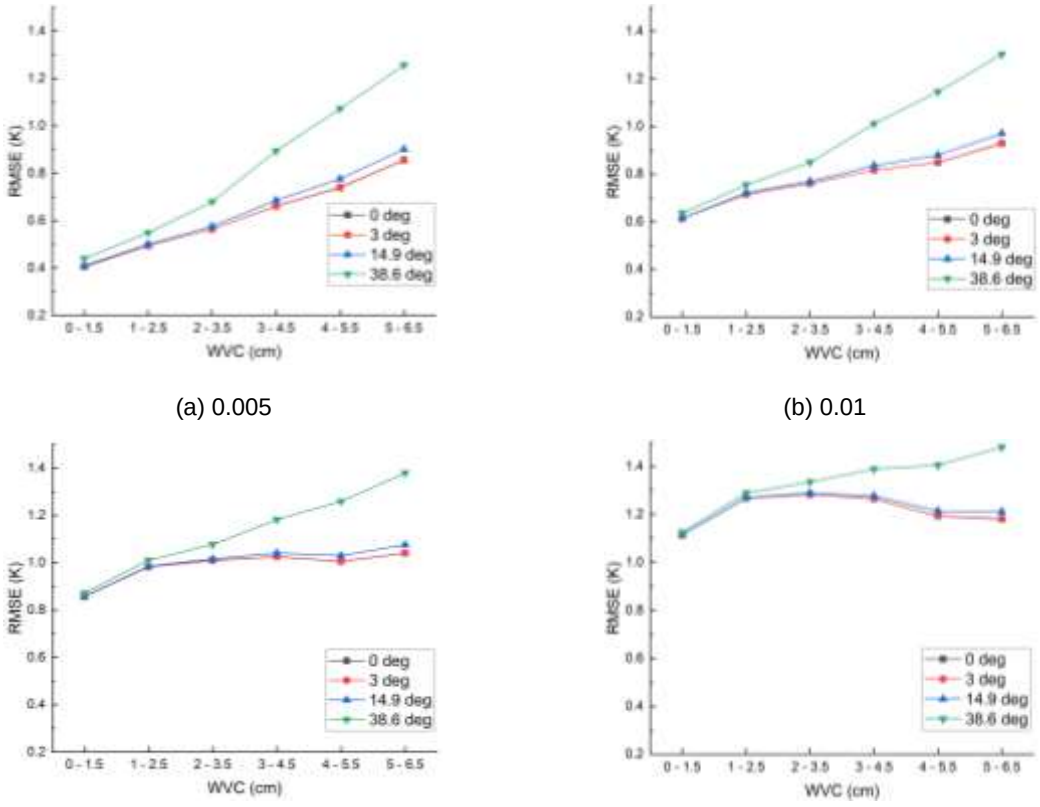

(a) 0.005 (b) 0.01

(c) 0.015 (d) 0.02

Figure 5.4. RMSE of LST estimates using the SW method with emissivity estimation noises of (a) 0.005, (b) 0.01, (c) 0.015 and (d) 0.02 for the daytime. The night-time is not shown considering its close performance to that of daytime.

5.4. SW quality control and diagnostics

The temperature and emissivity products will be assessed using a set of quality control (QC) flags. These flags will depend on ECOSTRESS radiance quality, emissivity data quality, whether the pixel is over land or water, the water vapour condition and cloud cover. The performance information in each step of the TES algorithm will also be provided in the QC flags to give users a summary of algorithm statistics. The QC flags are described using a 16-bit QC data. The structure of the QC data plane consists of six primary fields, which are detailed in Table 5.2:

1. Mandatory QC flags: overall description of status of pixel, produced with good quality, unreliable quality, not produced due to cloud or other reasons than cloud.

2. Radiance data quality field: good data, missing strip data and filled in, missing strip data and not filled in, not seen

3. Emissivity data quality field: within LSE uncertainty requirement (0.015)

4. Cloud mask and land/water mask field.

5. Water vapour condition.

Pixels with unreliable quality are typically either affected by cloud or high atmospheric water vapor content. These pixels usually have the emissivity in Band 5 < 0.95, or water vapour content >4.5.

Table 5.2. Bit flags defined in the QC data for the EEH-SW method

Bits	Long name	Description
1&0	Mandatory QA flags	00 = Pixel produced, best quality 01 = Pixel produced, nominal quality. Either one or more of the following conditions are met: 1) emissivity in both bands 4 and 5 < 0.95, i.e. possible cloud contamination 2) high water vapor content (>4.5) 3) pixel falls on missing scan line in Bands 1 and 5 and are filled using spatial neural network 4) emissivity estimation uncertainty >0.015 10 = Pixel produced, but cloud detected 11 = Pixel not produced due to missing data
3&2	Radiance data quality flag	00 = good quality L1B radiance data 01 = missing stripe pixel and filled in 10 = missing stripe pixel and not filled in 11 = not seen
5&4	Emissivity estimation uncertainty	00 = [0,0.005) 01 = [0.005,0.01) 10 = [0.01,0.015] 11 = beyond LSE uncertainty requirement (>0.015)
7&6	Cloud mask and land/water mask	Not set. Check the L1B GEO and cloud mask products for this information
9&8	Water vapour condition	00 = very dry atmosphere (wvc <1.5 $g.cm^{-2}$) 01 = dry atmosphere (1.5 ≤ wvc <3 $g.cm^{-2}$) 10 = moist atmosphere (3 ≤ wvc <4.5 $g.cm^{-2}$) 11 = very moist atmosphere (wvc >4.5 $g.cm^{-2}$)
10	ASTER GED	0 = good quality data 1 = missing data, soil emissivity climatology filled with average bare soil emissivity
11	FVC	0 = good quality data 1 = missing data, emissivity filled with interpolated value
15 - 12	Not set	These four bits are reserved for additional information.

5.5. SW uncertainty estimation

5.5.1. Emissivity uncertainty

The emissivity uncertainty comes from two sources mainly, i.e. the spectral conversion and the vegetation cover method (VCM). The spectral conversion can also introduce uncertainties into the LSE estimates, especially for the conversion to ECOSTRESS Band 5 that has little overlap with the 5 ASTER TIR bands. The RMSE obtained in the band conversion process is used. Uncertainties in bare ground emissivity, vegetation emissivity and FVC data

altogether contribute to the VCM uncertainty. The bare ground emissivity is provided in the ASTER GED data estimated using the TEUSim (Hulley et al. 2012). Based on Equation 5.5, the uncertainties in the VCM with respect to vegetation emissivity uncertainty, bare ground emissivity uncertainty and FVC uncertainty together can be expressed as

$$\delta\varepsilon_{VCM} = [f^2{\delta\varepsilon_v}^2 + (1-f)^2{\delta\varepsilon_g}^2 + (\varepsilon_v - \varepsilon_g)^2\delta f^2]^{1/2} \quad (5.7)$$

where f is FVC, $\delta\varepsilon_{VCM}$ is the VCM uncertainty, $\delta\varepsilon_v$, $\delta\varepsilon_g$, and δf are the uncertainties in vegetation emissivity, bare ground emissivity and FVC data, respectively. The final uncertainty is estimated as

$$\delta\varepsilon = [{\delta\varepsilon_{VCM}}^2 + {\delta\varepsilon_{CON}}^2]^{1/2} \quad (5.8)$$

where $\delta\varepsilon$ is the final emissivity uncertainty estimate, $\delta\varepsilon_{CON}$ is the spectral conversion uncertainty.

For pixels covered by snow, the VCM uncertainty is different from vegetated surfaces, expressed as

$${\delta\varepsilon_{VCM}}' = [{f_s}^2{\delta\varepsilon_{VCM}}^2 + (1-f_s)^2{\delta\varepsilon_s}^2 + (\varepsilon_{VCM} - \varepsilon_s)^2{\delta f_s}^2]^{1/2} \quad (5.9)$$

where $\delta\varepsilon_{VCM}$ is the VCM uncertainty over vegetated surfaces, f_s is the snow fractional cover, ε_s is the snow emissivity.

5.5.2. LST uncertainty

The LST uncertainty in the SW method can be mainly attributed to model uncertainty, emissivity uncertainty, measurement noise, and water vapor uncertainty. Similar to the uncertainty estimation for the TES algorithm, the SW uncertainty can be expressed as

$$\delta LST_{TES} = [{\delta LST_M}^2 + {\delta LST_E}^2 + {\delta LST_N}^2 + {\delta LST_W}^2]^{1/2} \quad (5.10)$$

where δLST_M, δLST_E, δLST_N, and δLST_W are the uncertainty from the SW model, emissivity estimation, measurement noise and water vapor content, respectively.

The same simulation data set as in Section 4.5 is built using SeeBor V5.0 profiles, emissivity spectrum library and the RTTOV atmospheric radiative transfer model. To calculate the separate contributions from each of these errors, the WVC, emissivity and TOA radiance are denoted as x = *TCW*, y = [ε_4, ε_5] and z = $L_\lambda(\theta)$. In the estimation, some errors are normally associated with the WVC used to find the corresponding SW coefficients, estimated emissivity

in Bands 4 and 5, and observed TOA radiance, written as $\hat{x} = x + \delta x$, $\hat{y} = y + \delta y$, and $\hat{z} = z + \delta z$. The emissivity uncertainties in Bands 4 and 5 are regarded as the same. The model uncertainty can be expressed as

$$\delta LST_M = E[(f(x,y,z) - LST_{sim})^2|_{x,y,z}]^{1/2}. \quad (5.11)$$

where $f(x,y,z)$ is the input data without errors and LST_{sim} is the LST used in the simulation. The emissivity uncertainty is set in the range between 0 and 0.015 with a bin of 0.003. The uncertainty in water vapour retrievals is estimated to be between 10% - 20%. Thus, the water vapor uncertainty is simulated using a random number generator with a mean of 15%. The measurement noise is added to the TOA radiance directly using a random number generator with a mean centred on the ECOSTRESS NE∆T. The LST uncertainty for each error source is estimated using the differences between the LST estimates with and without the corresponding error. The LST uncertainty is finally parameterised as follows:

$$\delta LST = a_0 + a_1 TCW + a_2 VZA + a_3 \delta\varepsilon + a_4 TCW.VZA + a_5 TCW.\delta\varepsilon + a_6 \delta\varepsilon.VZA + a_7 TCW^2 + a_8 VZA^2 + a_9 \delta\varepsilon^2 + a_{10} TCW.VZA.\delta\varepsilon \quad (5.12)$$

where a_i are the regressed coefficients, and TCW, VZA and $\delta\varepsilon$ are the water vapour content, viewing zenith angle and emissivity uncertainty, respectively.

5.6. SW algorithm output

The SW temperature and emissivity products will be archived in Hierarchical Data Format 5 – Earth Observing System (HDF5-EOS) format files. The scientific variable arrays in the EEH-SW product are listed in Table 5.3, including descriptions of data type, units, valid range, fill value, scale factor and offset. The variables include LST and estimated error, emissivity for the 2 bands used and associated errors, QC data plane and precipitable water vapour content. The data types and scaling factors have been optimized to minimize the amount of memory required to store the data.

Table 5.3. The scientific data sets (SDSs) for the EEH-SW product

SDS	Long name	Data type	Unit	Valid range	Fill value	Scale factor	Offset
LST	land surface temperature	unit16	K	7500-65535	0	0.02	0.0
LST_Err	land surface temperature error	unit8	K	1-255	0	0.04	0.0
Emis4	Band 4 emissivity	unit8	n/a	1-255	0	0.002	0.49

Emis5	Band 5 emissivity	unit8	n/a	1-255	0	0.002	0.49
Emis4_Err	Band 4 emissivity error	unit16	n/a	0-65535	0	0.0001	0.0
Emis5_Err	Band 5 emissivity error	unit16	n/a	0-65535	0	0.0001	0.0
QC	Quality control for LST and emissivity	unit16	n/a	0-65535	0	n/a	n/a
PWV	Precipitable water vapor	unit16	cm	0-65535	0	0.001	0.0

Acknowledgement

The research was carried out at the Luxembourg Institute of Science and Technology, under a contract with the European Space Agency.

6. Reference

Ackerman, S., Strabala, K., Menzel, P., Frey, R., Moeller, C., Gumley, L., Baum, B., Schaaf, C., & Riggs, G. (2010). Discriminating clear-sky from cloud with modis algorithm theoretical basis document (mod35). In: NASA

Baldridge, A.M., Hook, S.J., Grove, C.I., & Rivera, G. (2009). The ASTER spectral library version 2.0. *Remote sensing of Environment, 113*, 711-715

Borbas, E., Seemann, S.W., Huang, H.-L., Li, J., & Menzel, W.P. (2005). Global profile training database for satellite regression retrievals with estimates of skin temperature and emissivity. In (pp. 763-770)

Fisher, J.B., Lee, B., Purdy, A.J., Halverson, G.H., Dohlen, M.B., Cawse-Nicholson, K., Wang, A., Anderson, R.G., Aragon, B., & Arain, M.A. (2020). ECOSTRESS: NASA's next generation mission to measure evapotranspiration from the International Space Station. *Water Resources Research, 56*, e2019WR026058

Gao, C., Tang, B.-H., Wu, H., Jiang, X., & Li, Z.-L. (2013). A generalized split-window algorithm for land surface temperature estimation from MSG-2/SEVIRI data. *International Journal of Remote Sensing, 34*, 4182-4199

García-Santos, V., Coll, C., Valor, E., Niclòs, R., & Caselles, V. (2015). Analyzing the anisotropy of thermal infrared emissivity over arid regions using a new MODIS land surface temperature and emissivity product (MOD21). *Remote sensing of Environment, 169*, 212-221

Gillespie, A., Rokugawa, S., Matsunaga, T., Cothern, J.S., Hook, S., & Kahle, A.B. (1998). A temperature and emissivity separation algorithm for Advanced Spaceborne Thermal Emission and Reflection Radiometer (ASTER) images. *IEEE Transactions on Geoscience and Remote Sensing, 36*, 1113-1126

Hu, T., Cao, B., Du, Y., Li, H., Wang, C., Bian, Z., Sun, D., & Liu, Q. (2017). Estimation of surface upward longwave radiation using a direct physical algorithm. *IEEE Transactions on Geoscience and Remote Sensing, 55*, 4412-4426

Hu, T., Du, Y., Cao, B., Li, H., Bian, Z., Sun, D., & Liu, Q. (2016). Estimation of upward longwave radiation from vegetated surfaces considering thermal directionality. *IEEE Transactions on Geoscience and Remote Sensing, 54*, 6644-6658

Hu, T., Li, H., Cao, B., van Dijk, A.I.J.M., Renzullo, L.J., Xu, Z., Zhou, J., Du, Y., & Liu, Q. (2019). Influence of emissivity angular variation on land surface temperature retrieved using the generalized split-window algorithm. *International Journal of Applied Earth Observation and Geoinformation, 82*, 101917

Hulley, G., Hook, S., Fisher, J., & Lee, C. (2017). ECOSTRESS, A NASA Earth-Ventures Instrument for studying links between the water cycle and plant health over the diurnal cycle. In, *IEEE International Geoscience and Remote Sensing Symposium (IGARSS)* (pp. 5494-5496). Fort Worth, TX, USA: IEEE

Hulley, G.C., & Hook, S.J. (2008). A new methodology for cloud detection and classification with ASTER data. *Geophysical Research Letters, 35*

Hulley, G.C., & Hook, S.J. (2016a). ECOSTRESS Level-2 cloud detection algorithm theoretical basis document. In: JPL, California Institute of Technology

Hulley, G.C., & Hook, S.J. (2016b). ECOSTRESS Level-2 land surface temperature and emissivity algorithm theoretical basis document. In: JPL, California Institute of Technology

Hulley, G.C., Hook, S.J., Abbott, E., Malakar, N., Islam, T., & Abrams, M. (2015). The ASTER Global Emissivity Dataset (ASTER GED): Mapping Earth's emissivity at 100 meter spatial scale. *Geophysical Research Letters, 42*, 7966-7976

Hulley, G.C., Hughes, C.G., & Hook, S.J. (2012). Quantifying uncertainties in land surface temperature and emissivity retrievals from ASTER and MODIS thermal infrared data. *Journal of Geophysical Research: Atmospheres, 117*

Kustas, W., & Anderson, M. (2009). Advances in thermal infrared remote sensing for land surface modeling. *Agricultural and Forest Meteorology, 149*, 2071-2081

Li, H., Yang, Y., Li, R., Wang, H., Cao, B., Bian, Z., Hu, T., Du, Y., Sun, L., & Liu, Q. (2019). Comparison of the MuSyQ and MODIS Collection 6 land surface temperature products over

barren surfaces in the Heihe River Basin, China. *IEEE Transactions on Geoscience and Remote Sensing, 57*, 8081-8094

Li, Z.-L., Tang, B.-H., Wu, H., Ren, H., Yan, G., Wan, Z., Trigo, I.F., & Sobrino, J.A. (2013). Satellite-derived land surface temperature: Current status and perspectives. *Remote sensing of Environment, 131*, 14-37

Malakar, N.K., Hulley, G.C., Hook, S.J., Laraby, K., Cook, M., & Schott, J.R. (2018). An operational land surface temperature product for Landsat thermal data: Methodology and validation. *IEEE Transactions on Geoscience and Remote Sensing, 56*, 5717-5735

Mallick, K., Boegh, E., Trebs, I., Alfieri, J.G., Kustas, W.P., Prueger, J.H., Niyogi, D., Das, N., Drewry, D.T., & Hoffmann, L. (2015). Reintroducing radiometric surface temperature into the P enman-M onteith formulation. *Water Resources Research, 51*, 6214-6243

Mallick, K., Jarvis, A.J., Boegh, E., Fisher, J.B., Drewry, D.T., Tu, K.P., Hook, S.J., Hulley, G., Ardö, J., & Beringer, J. (2014). A Surface Temperature Initiated Closure (STIC) for surface energy balance fluxes. *Remote sensing of Environment, 141*, 243-261

Saunders, R., Matricardi, M., & Brunel, P. (1999). An improved fast radiative transfer model for assimilation of satellite radiance observations. *Quarterly Journal of the Royal Meteorological Society, 125*, 1407-1425

Shang, H., Chen, L., Letu, H., Zhao, M., Li, S., & Bao, S. (2017). Development of a daytime cloud and haze detection algorithm for Himawari-8 satellite measurements over central and eastern China. *Journal of Geophysical Research: Atmospheres, 122*, 3528-3543

Snyder, W.C., Wan, Z., Zhang, Y., & Feng, Y.Z. (1998). Classification-based emissivity for land surface temperature measurement from space. *International Journal of Remote Sensing, 19*, 2753-2774

Sobrino, J.A., Jiménez-Muñoz, J.C., Sòria, G., Ruescas, A.B., Danne, O., Brockmann, C., Ghent, D., Remedios, J., North, P., & Merchant, C. (2016). Synergistic use of MERIS and AATSR as a proxy for estimating Land Surface Temperature from Sentinel-3 data. *Remote sensing of Environment, 179*, 149-161

Sobrino, J.A., Raissouni, N., & Li, Z.-L. (2001). A comparative study of land surface emissivity retrieval from NOAA data. *Remote sensing of Environment, 75*, 256-266

Valor, E., & Caselles, V. (1996). Mapping land surface emissivity from NDVI: Application to European, African, and South American areas. *Remote sensing of Environment, 57*, 167-184

Wan, Z. (2014). New refinements and validation of the collection-6 MODIS land-surface temperature/emissivity product. *Remote sensing of Environment, 140*, 36-45

Wan, Z., & Dozier, J. (1996). A generalized split-window algorithm for retrieving land-surface temperature from space. *IEEE Transactions on Geoscience and Remote Sensing, 34*, 892-905

Wang, M., Zhang, Z., Hu, T., & Liu, X. (2019). A practical single-channel algorithm for land surface temperature retrieval: application to Landsat series data. *Journal of Geophysical Research: Atmospheres, 124*, 299-316

Yu, Y., Liu, Y., Yu, P., & Wang, H. (2017a). Enterprise algorithm theoretical basis document for VIIRS land surface temperature production. *NOAA: Silver Spring, MD, USA*

Yu, Y., Tarpley, D., Privette, J.L., Goldberg, M.D., Raja, M.K.R.V., Vinnikov, K.Y., & Xu, H. (2008). Developing algorithm for operational GOES-R land surface temperature product. *IEEE Transactions on Geoscience and Remote Sensing, 47*, 936-951

Yu, Y., Wang, H., Liu, Y., & Yu, P. (2017b). Enterprise land surface emissivity algorithm theoretical basis document. *NOAA*